Arrow of Time in Active Fluctuations

Édgar Roldán[1,2], Jérémie Barral[3,4], Pascal Martin[3,4], Juan M. R. Parrondo[5], and Frank Jülicher[2]
[1] *ICTP - The Abdus Salam International Centre for Theoretical Physics, Strada Costiera 11, 34151, Trieste, Italy*
[2] *Max Planck Institute for the Physics of Complex Systems, Nöthnitzer Str. 38, 01187 Dresden, Germany*
[3] *Laboratoire Physico-Chimie Curie, Institut Curie, PSL Research University, CNRS, UMR168, F-75248 Paris, France*
[4] *Sorbonne Université, UPMC Univ Paris 06, F-75252 Paris, France*
[5] *Departamento de Estructura de la Materia, Física Termica y Electronica and GISC, Universidad Complutense de Madrid 28040 Madrid, Spain*

We introduce lower bounds for the rate of entropy production of an active stochastic process by quantifying the irreversibility of stochastic traces obtained from mesoscopic degrees of freedom. Our measures of irreversibility reveal signatures of time's arrow and provide bounds for entropy production even in the case of active fluctuations that have no drift. We apply these irreversibility measures to experimental spontaneous hair-bundle oscillations from the ear of the bullfrog.

PACS numbers: 05.70.Ln, 87.16.dj, 05.40.-a

Active systems are maintained out of equilibrium by processes that consume resources of energy and produce entropy. This is the case of living cells, where energy is provided in the form of biochemical fuel such as adenosine triphosphate that drives active mesoscopic cellular processes. An important example of active cellular fluctuations are spontaneous oscillations of mechanosensory hair bundles of auditory hair cells [1, 2]. These oscillations have been proposed to amplify sound stimuli in the ear of many vertebrates, providing exquisite sensitivity and sharp frequency selectivity [3].

Active mesoscopic processes do not obey the fluctuation-dissipation theorem: measuring both the linear response of the system to weak external stimuli and spontaneous fluctuations provides a means to quantify deviations from thermal equilibrium [4–9]. A related important question is how entropy production can be estimated in active mesoscopic systems. In cases where active systems generate movement with drift, such as molecular motors moving along filaments [10–12], the rate of entropy production can be estimated from measurements of drift velocities and viscous forces [10, 13]. However, for active fluctuations without drift, such as spontaneous oscillations, it is unclear how entropy production can be characterized. Time irreversibility is a signature of the nonequilibrium nature of a system [14]. This suggests that quantification of irreversibility of fluctuations provides information about entropy production.

In this Letter, we introduce a hierarchy of bounds for the steady-state rate of entropy production based on measures of irreversibility of sets of mesoscopic observables. We show that quantifying irreversibility can reveal whether a noisy signal is produced by an active process or by a passive system. We apply the theory to experimental recordings of spontaneous mechanical oscillations of mechanosensory hair bundles in an excised preparation from the ear of the bullfrog (*Rana catesbeiana*) [15]. Our measures of irreversibility provide lower bounds for entropy production of active processes, as we demonstrate using a biophysical model for hair-bundle oscillations and experimental data.

We first discuss the relation between entropy production and irreversibility for generic nonequilibrium stationary processes. Consider a physical system described by a set of variables labeled as X_α, with $\alpha = 1, 2, \dots$. In a stationary nonequilibrium process of time duration t, the physical system traces a trajectory in the phase space described by the stochastic processes $X_\alpha(t)$. We denote by $\mathbf{\Gamma}_{[0,t]} \equiv \{(x_1(s), x_2(s), \dots)\}_{s=0}^t$ a given trajectory described by the system variables and its corresponding time-reversed trajectory as $\widetilde{\mathbf{\Gamma}}_{[0,t]} \equiv \{(\theta_1 x_1(t-s), \theta_2 x_2(t-s), \dots)\}_{s=0}^t$, where $\theta_\alpha = \pm 1$ is the time-reversal signature of the $\alpha-$th variable. Assume now that X_α are the variables that may be out of equilibrium, i.e. we do not include in $\mathbf{\Gamma}_{[0,t]}$ those variables corresponding to thermal reservoirs, chemostats, etc. In that case, the steady-state rate of entropy production $\sigma_{\rm tot}$ is given by

$$\sigma_{\rm tot} = k_{\rm B} \lim_{t\to\infty} \frac{1}{t} D\left[\mathcal{P}\left(\mathbf{\Gamma}_{[0,t]}\right) \Big|\Big| \mathcal{P}\left(\widetilde{\mathbf{\Gamma}}_{[0,t]}\right)\right] \quad , \qquad (1)$$

where $k_{\rm B}$ is the Boltzmann constant and $\mathcal{P}$ denotes the steady-state path probability [16–19]. Here $D[\mathcal{Q}||\mathcal{R}] \geq 0$ is the Kullback-Leibler (KL) divergence between the probability measures $\mathcal{Q}$ and $\mathcal{R}$, which quantifies the distinguishability between these two distributions. For measures of a single random variable x the KL divergence is given by $D[\mathcal{Q}(x)||\mathcal{R}(x)] \equiv \int {\rm d}x\, \mathcal{Q}(x) \ln[\mathcal{Q}(x)/\mathcal{R}(x)]$. Note that for isothermal systems $\sigma_{\rm tot} T$ equals to the rate of heat dissipated to the environment at temperature T.

Often in experiments only one or several of the nonequilibrium variables can be tracked in time. Consider the case where only $X_1, \dots X_k$ are known. We define the $k-$variable rate of entropy production in terms of path probabilities of k mesoscopic variables

$$\sigma_k \equiv k_{\rm B} \lim_{t\to\infty} \frac{1}{t} D\left[\mathcal{P}\left(\mathbf{\Gamma}^{(k)}_{[0,t]}\right) \Big|\Big| \mathcal{P}\left(\widetilde{\mathbf{\Gamma}}^{(k)}_{[0,t]}\right)\right] \quad , \qquad (2)$$

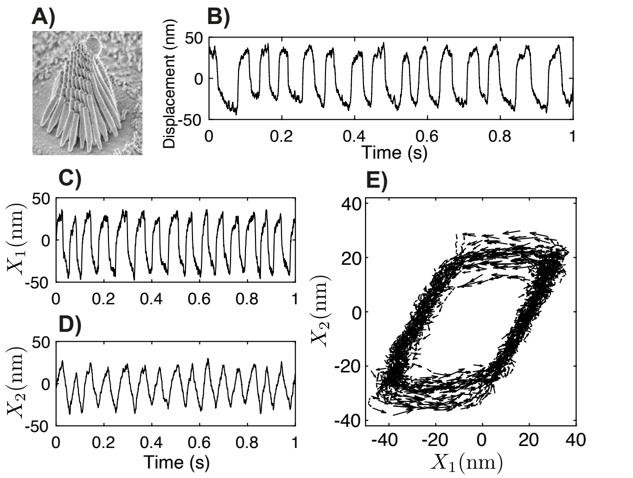

FIG. 1: **(A)** Electron micrograph of a hair-cell bundle extracted from the bullfrog's inner ear. The distance from top to bottom is $\sim 7\mu$m. **(B)** Experimental recording of the tip position of an active mechanosensory hair bundle that displays spontaneous oscillations. **(C,D)** Trajectories of the reduced variables X_1 (C) and X_2 (D) as a function of time obtained from a simulation of the stochastic model given by Eqs. (3-4). **(E)** Representation of a 2-s trace of the simulations in (C,D) in the $\{X_1(t), X_2(t)\}$ plane. The black arrows illustrate the value of the instantaneous velocity and the base of the arrow the position. Parameters of the simulations: $\lambda_1 = 0.9\,$pNms/nm, $\lambda_2 = 5\,$pNms/nm, $k_{\rm gs} = 0.55\,$pN/nm, $k_{\rm sp} = 0.3\,$pN/nm, $D = 72\,$nm, $S = 0.73$, $F_{\rm max} = 45.76\,$pN, $N = 50$, $\Delta G = 10 k_{\rm B}T$, $k_{\rm B}T = 4.143\,$pNnm and $T_{\rm eff}/T = 1.5$.

where $\mathbf{\Gamma}_{[0,t]}^{(k)} \equiv \{(x_1(s),\dots,x_k(s))\}_{s=0}^t$ and $\widetilde{\mathbf{\Gamma}}_{[0,t]}^{(k)} \equiv \{(\theta_1 x_1(t-s),\dots,\theta_k x_k(t-s))\}_{s=0}^t$ denote paths described by k variables. The average $k-$variable rate of entropy production increases with the number of tracked degrees of freedom $0 \leq \sigma_1 \leq \dots \leq \sigma_k \leq \sigma_{k+1} \leq \dots \leq \sigma_{\rm tot}$. It can also be shown that the estimator σ_k equals the physical entropy production $\sigma_{\rm tot}$ if the missing variables, X_ℓ with $\ell > k$, are at thermal equilibrium [20–22]. When the missing variables are not at thermal equilibrium, which is often the case in active systems, the estimator $\sigma_k \leq \sigma_{\rm tot}$ yields only a lower bound for the entropy production rate.

We now discuss irreversibility and entropy production in active mechanosensory hair cells from the bullfrog's ear. Hair cells work as cellular microphones that transduce mechanical vibrations evoked by sound into electrical signals [23]. They are endowed with a tuft of cylindrical protrusions −the hair bundle (Fig. 1A)− that serves both as sensory antenna and as active oscillator that amplifies sound [3]. In experimental recordings of spontaneous hair-bundle oscillations, only the tip position X_1 of the bundle is measured (Fig. 1B). Measuring X_1, we can only estimate σ_1, which provides a lower bound to the total steady-state entropy production rate $\sigma_{\rm tot}$.

Spontaneous hair-bundle oscillations are thought to result from an interplay between opening and closing of mechanosensitive ion channels, activity of molecular motors that pull on the channels, and fast calcium feedback. This interplay can be described by two coupled stochastic differential equations for the position of the bundle X_1 and of the motors X_2 [2, 15, 24]:

$$\lambda_1 \dot{X}_1 = -\frac{\partial V}{\partial X_1} + \sqrt{2k_{\rm B}T\lambda_1}\,\xi_1 \qquad (3)$$

$$\lambda_2 \dot{X}_2 = -\frac{\partial V}{\partial X_2} - F_{\rm act} + \sqrt{2k_{\rm B}T_{\rm eff}\lambda_2}\,\xi_2 \quad , \qquad (4)$$

where λ_1 and λ_2 are friction coefficients and ξ_1 and ξ_2 in (3-4) are two independent Gaussian white noises with zero mean $\langle \xi_i(t)\rangle = 0$ $(i = 1,2)$ and correlation $\langle \xi_i(t)\xi_j(t')\rangle = \delta_{ij}\delta(t-t')$, with $i,j = 1,2$ and δ_{ij} the Kronecker's delta. T is the temperature of the environment, whereas the parameter $T_{\rm eff} > T$ is an effective temperature that characterizes fluctuations of the motors. The conservative forces derive from the potential associated with elastic elements and mechano-sensitive ion channels

$$V(X_1,X_2) = \frac{k_{\rm gs}\Delta X^2 + k_{\rm sp}X_1^2}{2} + Nk_{\rm B}T\ln\left[\exp\left(\frac{k_{\rm gs}D\Delta X}{Nk_{\rm B}T}\right) + A\right] \quad , \qquad (5)$$

where $\Delta X = X_1 - X_2$; $k_{\rm gs}$ and $k_{\rm sp}$ are stiffness coefficients; D is the gating swing of a transduction channel; and $A = \exp[(\Delta G + (k_{\rm gs}D^2)/2N)/(k_{\rm B}T)]$, ΔG being the energy difference between open and closed states of the channels and N the number of transduction elements. The force $F_{\rm act}(X_1,X_2) = F_{\rm max}(1 - SP_{\rm o}(X_1,X_2))$ is an active nonconservative force exerted by the molecular motors with a maximum value $F_{\rm max}$. The parameter S quantifies calcium-mediated feedback on the motor force [25] and $P_{\rm o}(X_1,X_2) = 1/[1 + A\exp(-k_{\rm gs}D\Delta X/Nk_{\rm B}T)]$ is the open probability of the transduction channels. With this model, we can capture key features of noisy spontaneous oscillations of hair-bundle position X_1 that have been observed experimentally (Fig. 1C and D). The oscillation of the motors' position (Fig. 1D) is known in the model but hidden in experiments. Trajectories of only $X_1(t)$ or $X_2(t)$ do not reveal obvious signs of a net current, which here would correspond to a drift. However, trajectories in the (X_1,X_2) plane show a net current which is a signature of entropy production (Fig. 1E). In the following, we will use this stochastic model to compare the irreversibility measure σ_1 to the total entropy production $\sigma_{\rm tot}$.

In the stochastic model of hair-bundle oscillations given by Eqs. (3-4) we deal with only two variables, therefore $\sigma_{\rm tot} = \sigma_2$. From the analytical expression of σ_2, we find that the steady-state entropy production rate can be written as [26, 27]

$$\sigma_{\rm tot} = -\langle \dot{Q}_1\rangle\left(\frac{1}{T} - \frac{1}{T_{\rm eff}}\right) + \frac{\langle \dot{W}_{\rm act}\rangle}{T_{\rm eff}} \quad , \qquad (6)$$

where $-\langle \dot{Q}_1 \rangle = -\langle (\partial V/\partial X_1) \circ \dot{X}_1 \rangle$ is the steady-state average heat dissipated to the thermal bath at temperature T and $\langle \dot{W}_{\rm act} \rangle = -\langle F_{\rm act} \circ \dot{X}_2 \rangle$ is the power exerted by the active force on the motors. Here $\langle \cdot \rangle$ denote steady state averages and $\circ$ the Stratonovich product [28, 29]. Equation (6) reveals two sources of nonequilibrium in the model: the difference of effective temperature and temperature, and the active force.

We now introduce a new method to estimate the irreversibility measure σ_1 for any nonequilibrium steady state from a single stationary time series $x_i = X(i\Delta t)$ ($i = 1, \ldots, n$) of a variable X that is even under time reversal. We describe the technique for a single variable, but it can be generalized to several variables $X_\alpha(t)$. In discrete processes, the KL divergence in σ_1 can be accurately measured from the statistics of sequences of symbols [30, 31]. In continuous processes however, estimating σ_1 is a herculean task due to the difficulties in sampling the whole phase space of paths [32–34].

The key idea of our method is to exploit the invariance of the KL divergence under one-to-one transformations. Suppose that there exists a one-to-one map $\xi_i(x_1, \ldots, x_n)$, $i = 1, \ldots, n$, that transforms the original time series and its time reversal into two new time series $\xi_i^F = \xi_i(x_1, \ldots, x_n)$ and $\xi_i^R = \xi_i(x_n, \ldots, x_1)$ that are independent and identically distributed (i.i.d.) processes. Such a procedure is often called a *whitening* filter [35, 36]. Because the new series are i.i.d., the KL divergence is now simple to calculate: it is given by the KL divergence between two *univariate* distributions $p(\xi)$ and $q(\xi)$, corresponding to the stationary probability distribution of ξ_i^F and ξ_i^R, respectively [34]. In general, it is not possible to find a one-to-one map that fully eliminates the correlations of both the forward $(x_1, \ldots, x_n)$ and the backward $(x_n, \ldots, x_1)$ time series. In that case, the removal of the correlations in the backward series is enough to provide a lower bound for σ_1:

$$\sigma_1 \geq k_{\rm B} f_{\rm s} D[p(\xi)||q(\xi)] \equiv \hat{\sigma}_1 \quad , \tag{7}$$

where $f_{\rm s} = (\Delta t)^{-1}$ is the sampling frequency and $D[p(\xi)||q(\xi)] = \int {\rm d}\xi\, p(\xi) \ln[p(\xi)/q(\xi)]$ is the KL divergence between the univariate distributions $p(\xi)$ and $q(\xi)$. We estimate $D[p(\xi)||q(\xi)] \simeq \gamma \sum_i \hat{p}_i \ln(\hat{p}_i/\hat{q}_i)$ where $\hat{p}, \hat{q}$ are empirical densities, and the sum runs over the number of histogram bins. We introduce the prefactor $\gamma = 1 - p_{\rm KS} \leq 1$, where $p_{\rm KS}$ is the p-value of the Kolmogorov-Smirnov statistic between $p(\xi)$ and $q(\xi)$, to correct the statistical bias of our KL divergence estimate [37]. The proof of the bound (7) and further details of the estimate are found in [29].

In the following, we make use of autoregressive (AR) models for the whitening transformation. More precisely, we obtain the transformed time series ξ_i^F (ξ_i^R) as the difference between the observed values of the forward (backward) time series and the forecast of that value based on an AR model of order $m = 10$. Parameters of the model are determined from fits of the AR-model to the time-reversed series of positions.

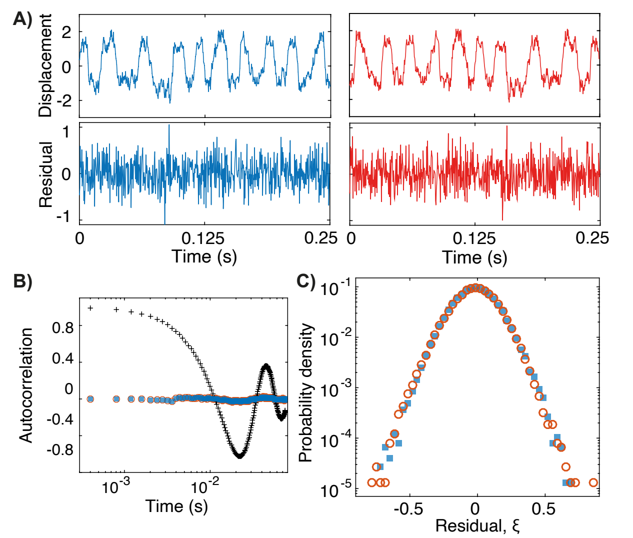

FIG. 2: Illustration of the method to quantify time irreversibility $\hat{\sigma}_1$ from an experimentally obtained stochastic time series x_i of the tip position of a hair bundle partially shown in top left panel in (A) (blue line). **(A)** Top: Time series (top left, blue line) and time-reversed series (top right, red line) normalized by their standard deviation. Bottom: residual time series ξ_i^F (bottom left, blue line), ξ_i^R (bottom right, red line) given by the difference between the original series and their predictions from an autoregressive model of order 10 fitted to the time-reversed series. **(B)** Autocorrelation function of the forward time series x_i (black "+"), and the residual time series ξ_i^F (blue filled squares) and ξ_i^R (red open circles). **(C)** Empirical probability densities of the time series ξ_i^F ($p(\xi)$, blue filled squares) and ξ_i^R ($q(\xi)$, red open circles). The data corresponds to a 30-s recording of the tip position of an active hair bundle with oscillation frequency $f_{\rm o} = 23\,$Hz and sampling rate $f_{\rm s} = 2.5\,$kHz.

Figure 2 illustrates our estimate of σ_1 applied to a representative experimental time series of hair-bundle oscillations, plotted in panel A (top left). The residual time series ξ_i^F and ξ_i^R (Fig. 2A, bottom) obtained from the whitening transformation barely have any time correlation (Fig. 2B) and are therefore i.i.d. processes in good approximation. Although the time series and its time reversed (Fig. 2A, top right) do not look different by eye, corresponding to relatively low values of the Kolmogorov-Smirnov p-value (here $p_{\rm KS} = 0.06$), the measure provided by the KL divergence (Eq. 7) yields $\hat{\sigma}_1 = (4.3 \pm 0.8) k_{\rm B}/{\rm s}$ revealing that the residual distributions $p(\xi)$ and $q(\xi)$ are different (Fig. 2C), i.e. time irreversibility. Since $\sigma_{\rm tot} \geq \sigma_1 \geq \hat{\sigma}_1$, Eq. (7) implies that our irreversibility measure $\hat{\sigma}_1$ provides for this case the bound $\sigma_{\rm tot} \geq (4.3 \pm 0.8) k_{\rm B}/{\rm s}$ for the rate of entropy production. This bound corresponds to an entropy production rate of at least $(0.19 \pm 0.03) k_{\rm B}$ per oscillation cycle [29]. Interestingly, this value corresponds to a rate of heat dissipation that

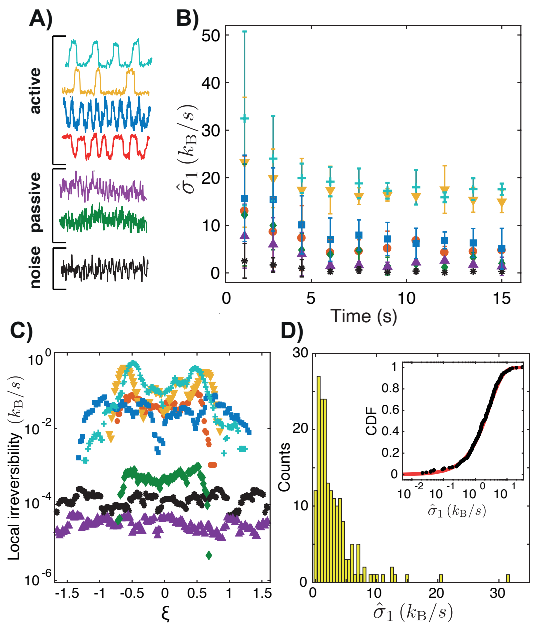

FIG. 3: **(A)** Examples of experimental traces for the tip position of different mechanosensory hair bundles as a function of time. Top: active hair bundles. Bottom: passive hair bundles, i.e. when the channel blocker gentamicin is present (magenta, green), and experimental noise trace (black). The data used in Fig. 2 corresponds to the oscillation shown here in red. **(B)** Irreversibility measure $\hat{\sigma}_1$ (symbols) as a function of the observation time obtained from the experimental traces partially shown in (A). **(C)** Estimate of the local irreversibility measure (8) obtained from single 30s recordings of the oscillations shown in panel A as a function of the residual value ξ. **(D)** Histogram of the irreversibility measure $\hat{\sigma}_1$ obtained from 182 experimental recordings of spontaneous active oscillations of the hair bundle of duration $t_{\rm exp} = 30\,$s. The experimental average value of the irreversibility measure $\hat{\sigma}_1$ is $\sim 3k_{\rm B}/s$. Inset: Empirical cumulative distribution function (CDF) of irreversibility (black circles). The red line is a fit to an exponential distribution with mean value $(2.82{\pm}0.02)k_{\rm B}/s$ and $R^2 > 0.9990$. The sampling rate was $f_{\rm s} = 2.5\,$kHz.

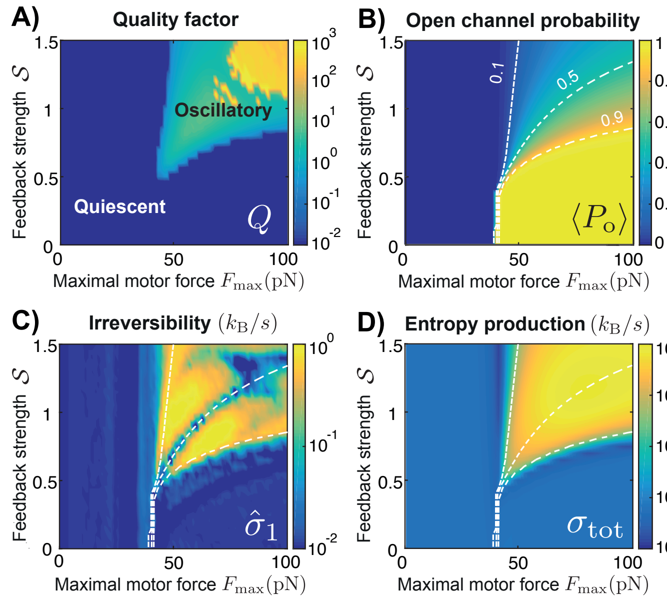

FIG. 4: Dynamical and thermodynamic features of spontaneous hair-bundle oscillations as a function the calcium-feedback strength S and maximal motor force $F_{\rm max}$ obtained from numerical simulations of the model given by Eqs. (3-4): **(A)** Quality factor Q; **(B)** Steady-state average of the open channel probability $\langle P_{\rm o}\rangle$; **(C)** Irreversibility measure $\hat{\sigma}_1$; **(D)** Steady-state entropy production rate $\sigma_{\rm tot}$. In (B,C,D) we indicate the parameter values for which $\langle P_{\rm o}\rangle = 0.1, 0.5$ and 0.9 (white dashed lines from top to bottom, respectively). The results are obtained from numerical simulations of Eqs. (3-4) of total duration $t_{\rm sim} = 300\,$s, sampling frequency $f_{\rm s} = 1\,$kHz and parameter values $\lambda_1 = 2.8\,$pNms/nm, $\lambda_2 = 10\,$pNms/nm, $k_{\rm gs} = 0.75\,$pN/nm, $k_{\rm sp} = 0.6\,$pN/nm, $D = 61\,$nm, $\Delta G = 10k_{\rm B}T$, $k_{\rm B}T = 4\,$pNnm and $T_{\rm eff}/T = 1.5$.

is below, here by two orders of magnitude, the estimated mean power output per hair cell $\sim 10k_{\rm B}T/$cycle found for spontaneous emissions of sound by the ears of lizards [38].

We apply our method to quantify irreversibility in active oscillatory hair bundles (Fig. 3A, top), in quiescent hair bundles exposed to a drug (gentamicin) that blocks the transduction channels (Fig. 3A, magenta and green) and for noisy signals produced by the recording apparatus when there is no hair bundle under the objective of the microscope (Fig. 3A, black). For sufficiently long recordings, $\hat{\sigma}_1$ saturates to a value that exceeds the value obtained for cells exposed to gentamicin and for experimental noise (Fig. 3B). To gain further insights, we apply the local irreversibility measure

$$\hat{s}_1(\xi) \equiv k_{\rm B} f_{\rm s}\left[p(\xi)\ln\frac{p(\xi)}{q(\xi)} + q(\xi) - p(\xi)\right] \quad , \qquad (8)$$

which obeys $\hat{s}_1(\xi) \geq 0$ for all ξ [39], and $\hat{\sigma}_1 = \int {\rm d}\xi \hat{s}_1(\xi)$: for all the analyzed values of ξ, the local irreversibility of active oscillations is $\sim 10^3$ times larger than for passive oscillations and experimental noise. Using a population of 182 hair cells that showed spontaneous hair-bundle oscillations [15], we obtained a probability density of $\hat{\sigma}_1$ that was well described by an exponential distribution with mean $3\,k_{\rm B}$/s (Fig. 3C). Interestingly, this result depends on the sampling frequency $f_{\rm s}$: irreversibility is maximal in the range $f_{\rm s} \sim (200-600)$Hz where its value goes up to $4.3\,k_{\rm B}$/s. This frequency dependency may provide additional information about timescales of the underlying active process [29].

Finally, we relate these estimates of entropy production from experimental recordings to results obtained for a stochastic model of hair-bundle oscillations. We performed numerical simulations of Eqs. (3-4) for different values of the control parameters $F_{\rm max}$ and S (Fig. 4) to explore entropy production throughout the state diagram of the system. The quality factor of the oscillation Q −given by the ratio between the oscillation frequency and the bandwidth at half the maximal height of the power spectrum− and the average open probability $\langle P_o \rangle$ at steady state are displayed in Fig. 4A-B in the state diagram. The irreversibility measure $\hat{\sigma}_1$ for trajectories $X_1(t)$ of spontaneous oscillations is shown in Fig. 4C. This measure can be compared to the quantification of total entropy production σ_{tot} of the model, given by Eq. (6), which is shown in Fig. 4D. Irreversibility of trajectories and total entropy production correlate strongly. However, as expected, $\hat{\sigma}_1$ provides a lower bound: the rate of entropy production estimated from our measure is here typically three orders of magnitude smaller than the total entropy production. Clearly, measuring other degrees of freedom additional to the hair-bundle position would be required to obtain tighter bounds to the rate of entropy production with our method or other estimation techniques [40–44].

In summary, we have shown that fluctuations of active systems can reveal the arrow of time even in the absence of net drifts or currents. The hierarchy of measures of time irreversibility introduced here provides lower bounds for the entropy production of an active process. These irreversibility measures can quantify contributions to entropy production in active matter, including living systems, from fluctuations of only a few mesoscopic degrees of freedom. We have here demonstrated the applicability of the approach by estimating entropy production associated with experimental noisy oscillations of a single degree of freedom in the case of mechanosensory hair bundles from the bullfrog's ear.

We thank Peter Gillespie for providing the hair-bundle picture used in Fig. 1A. We acknowledge stimulating discussions with Izaak Neri, Andre C. Barato, Simone Pigolotti, Johannes Baumgart, Jose Negrete Jr, Ken Sekimoto, Ignacio A. Martínez, Patrick Pietzonka and A.J. Hudspeth.

[1] P. Martin, D. Bozovic, Y. Choe, and A. Hudspeth, J. Neurosci. **23**, 4533 (2003).
[2] J.-Y. Tinevez, F. Jülicher, and P. Martin, Biophys. J. **93**, 4053 (2007).
[3] A. Hudspeth, Nature Rev. Neurosci. **15**, 600 (2014).
[4] P. Martin, A. Hudspeth, and F. Jülicher, PNAS **98**, 14380 (2001).
[5] D. Mizuno, C. Tardin, C. F. Schmidt, and F. C. MacKintosh, Science **315**, 370 (2007).
[6] R. Rodríguez-García, I. López-Montero, M. Mell, G. Egea, N. S. Gov, and F. Monroy, Biophys. J. **108**, 2794 (2015).
[7] H. Turlier, D. A. Fedosov, B. Audoly, T. Auth, N. S. Gov, C. Sykes, J. F. Joanny, G. Gompper, and T. Betz, Nature Phys. **12**, 513 (2016).
[8] C. Battle, C. P. Broedersz, N. Fakhri, V. F. Geyer, J. Howard, C. F. Schmidt, and F. C. MacKintosh, Science **352**, 604 (2016).
[9] C. Nardini, É. Fodor, E. Tjhung, F. Van Wijland, J. Tailleur, and M. E. Cates, Phys. Rev. X **7**, 021007 (2017).
[10] F. Jülicher, A. Ajdari, and J. Prost, Rev. Mod. Phys. **69**, 1269 (1997).
[11] D. Keller and C. Bustamante, Biophys. J. **78**, 541 (2000).
[12] J. Howard, *Mechanics of motor proteins and the cytoskeleton* (Sinauer associates Sunderland, MA, 2001).
[13] H. Qian, J. Math. Chem. **27**, 219 (2000).
[14] I. Z. Steinberg, Biophys. J. **50**, 171 (1986).
[15] J. Barral, F. Jülicher, and P. Martin, Biophys. J. **114**, 425 (2018).
[16] J. L. Lebowitz and H. Spohn, J. Stat. Phys. **95**, 333 (1999).
[17] C. Maes and K. Netočný, J. Stat. Phys. **110**, 269 (2003).
[18] U. Seifert, Phys. Rev. Lett. **95**, 040602 (2005).
[19] I. Neri, É. Roldán, and F. Jülicher, Phys. Rev. X **7**, 011019 (2017).
[20] A. Gomez-Marin, J. M. R. Parrondo, and C. Van den Broeck, EPL **82**, 50002 (2008).
[21] J. Mehl, B. Lander, C. Bechinger, V. Blickle, and U. Seifert, Phys. Rev. Lett. **108**, 220601 (2012).
[22] A. Celani, S. Bo, R. Eichhorn, and E. Aurell, Phys. Rev. Lett. **109**, 260603 (2012).
[23] A. J. Hudspeth, Nature **341**, 397 (1989).
[24] V. Bormuth, J. Barral, J.-F. Joanny, F. Jülicher, and P. Martin, PNAS **111**, 7185 (2014).
[25] B. Nadrowski, P. Martin, and F. Jülicher, PNAS **101**, 12195 (2004).
[26] R. Chetrite and K. Gawedzki, Comm. Math. Phys. **282**, 469 (2008).
[27] L. Dabelow, S. Bo, and R. Eichhorn, arXiv:1806.04956 (2018).
[28] K. Sekimoto, Prog. Theor. Phys. Suppl. **130**, 17 (1998).
[29] See Supplemental Material.
[30] E. Roldán and J. M. R. Parrondo, Phys. Rev. Lett. **105**, 150607 (2010).
[31] É. Roldán and J. M. R. Parrondo, Phys. Rev. E **85**, 031129 (2012).
[32] D. Andrieux, P. Gaspard, S. Ciliberto, N. Garnier, S. Joubaud, and A. Petrosyan, J. Stat. Mech. **2008**, P01002 (2008).
[33] S. Tusch, A. Kundu, G. Verley, T. Blondel, V. Miralles, D. Démoulin, D. Lacoste, and J. Baudry, Phys. Rev. Lett. **112**, 180604 (2014).
[34] E. Roldán, *Irreversibility and dissipation in microscopic systems* (Springer Theses, Berlin, 2014).
[35] A. J. Efron and H. Jeen, IEEE Trans. Sign. Proc. **42**, 1572 (1994).
[36] A. Galka, T. Ozaki, J. B. Bayard, and O. Yamashita, J. Stat. Phys. **124**, 1275 (2006).
[37] J. A. Bonachela, H. Hinrichsen, and M. A. Munoz, J. Phys. A **41**, 202001 (2008).
[38] G. A. Manley and L. Gallo, J. Acoust. Soc. Am. **102**, 1049 (1997).
[39] N. Shiraishi, K. Saito, and H. Tasaki, Phys. Rev. Lett. **117**, 190601 (2016).
[40] É. Roldán, I. Neri, M. Dörpinghaus, H. Meyr, and F. Jülicher, Phys. Rev. Lett. **115**, 250602 (2015).
[41] P. Pietzonka, A. C. Barato, and U. Seifert, Phys. Rev. E **93**, 052145 (2016).
[42] C. Maes, Phys. Rev. Lett. **119**, 160601 (2017).
[43] J. Li, J. M. Horowitz, T. R. Gingrich, and N. Fakhri, arXiv:1809.02118 (2018).
[44] A. Frishman and P. Ronceray, arXiv:1809.09650 (2018).
[45] F. Jülicher, K. Dierkes, B. Lindner, J. Prost, and P. Martin, Eur. Phys. J. E **29**, 449 (2009).

SUPPLEMENTAL MATERIAL

Here we present additional details of the methods and results discussed in the Main Text. In Secs. and , we provide a derivation of the bound used in Eq. (7) in the Main Text, and describe the whitening transformation that we use to estimate irreversibility of stochastic time traces. In Sec. , we provide further details on the experimental results and error analysis for the data shown in Fig. 2 in the Main Text. In Sec. , we provide further details on the experimental results reported in Fig. 3 in the Main Text. In Sec. , we analyze how our irreversibility measure depends on the data sampling rate of the experimental recordings of hair-bundle spontaneous fluctuations. In Sec. we introduce and describe the local irreversibility measure given by Eq. (8) in the Main Text. In Sec. , we discuss how entropy production is estimated in numerical simulations of the hair-bundle biophysical model. Section provides details on the calculation of the quality factor of spontaneous oscillations shown in Fig. 4A in the Main Text. In Sec. , we discuss the biophysical model of hair-bundle oscillations and the experimental techniques.

S1. BOUNDS ON THE MULTIVARIATE KULLBACK-LEIBLER DIVERGENCE

Here we prove a general lower bound for the Kullback-Leibler (KL) divergence between two multivariate probability densities $P_X(x_1,\dots,x_n)$ and $Q_X(x_1,\dots,x_n)$ that fulfill the following: there exits a one-to-one map $\xi_i = \xi_i(x_1,\dots,x_n)$ with $i = 1,\dots,n$, such that

1. the transformed variables ξ_i are identically distributed under both P and Q, that is, the distributions $P_\Xi(\xi_1,\dots,\xi_n)$ and $Q_\Xi(\xi_1,\dots,\xi_n)$ have, respectively, identical marginal distributions $p(\xi)$ and $q(\xi)$ for any ξ_i $(i = 1,\dots,n)$;
2. the transformed variables ξ_i are independent and identically distributed (i.i.d.) under the distribution Q, that is, $Q_\Xi(\xi_1,\dots,\xi_n) = \Pi_i\, q(\xi)$.

The first step in the derivation is a simple application of the invariance of the KL distance under a one-to-one map:

$$D\left[P_X(x_1,\dots,x_n)||Q_X(x_1,\dots,x_n)\right] = D\left[P_\Xi(\xi_1,\dots,\xi_n)||Q_\Xi(\xi_1,\dots,\xi_n)\right] \quad . \tag{S9}$$

Second, we can rewrite the relative entropy as

$$\begin{aligned} D\left[P_\Xi(\xi_1,\dots,\xi_n)||Q_\Xi(\xi_1,\dots,\xi_n)\right] &= \int \mathrm{d}\xi_1 \cdots \int \mathrm{d}\xi_n\, P_\Xi(\xi_1,\dots,\xi_n) \ln \frac{P_\Xi(\xi_1,\dots,\xi_n)}{\Pi_i\, q(\xi_i)} \\ &= \int \mathrm{d}\xi_1 \cdots \int \mathrm{d}\xi_n \left[P_\Xi(\xi_1,\dots,\xi_n) \ln \frac{\Pi_i\, p(\xi_i)}{\Pi_i\, q(\xi_i)} + P_\Xi(\xi_1,\dots,\xi_n) \ln \frac{P_\Xi(\xi_1,\dots,\xi_n)}{\Pi_i\, p(\xi_i)} \right] \\ &= nD[p(\xi)||q(\xi)] + D\left[P_\Xi(\xi_1,\dots,\xi_n)||\Pi_i\, p(\xi_i)\right] \quad . \end{aligned} \tag{S10}$$

Because the KL divergence between two distributions is always positive, Eqs. (S9) and (S10) yield the bound

$$D\left[P_X(x_1,\dots,x_n)||Q_X(x_1,\dots,x_n)\right] \geq nD[p(\xi)||q(\xi)] \quad , \tag{S11}$$

and the inequality saturates if the transformed variables ξ_i $(i = 1\dots n)$ are also i.i.d. under $P_\Xi(\xi_1,\dots,\xi_n)$, i.e. when $P_\Xi(\xi_1,\dots,\xi_n) = \Pi_i\, p(\xi_i)$. If one can find a one-to-one map that transforms the original random variables into i.i.d. variables under *both* distributions P and Q, then (S11) becomes an equality and the exact KL divergence between the two multivariate distributions P_X and Q_X can be reduced to the KL divergence between single variable distributions $p(\xi)$ and $q(\xi)$, which is much easier to evaluate from real data. This is the key idea of our method to estimate the irreversibility of experimental time series.

S2. IRREVERSIBILITY IN CONTINUOUS TIME SERIES: THE WHITENING TRANSFORMATION

The estimation of the KL divergence rate from single stationary trajectories of both discrete and continuous random variables have been previously discussed [34]. For continuous random variables, the most common strategy is to make a symbolization or discretization of the time series [32]. Then, the KL divergence is estimated from the statistics of substrings of increasing length [30, 31]. The main limitation of this method is that one easily reaches lack of statistics even for short substrings. If the observed time series is non-Markovian, this limitation could yield inaccurate bounds for the entropy production. For instance, the KL divergence between two data substrings can be zero in non-equilibrium stationary states without observable currents [30, 31, 34].

Here we introduce a new method to estimate the KL divergence rate

$$\frac{\sigma_1}{k_{\mathrm{B}}} \equiv \lim_{t\to\infty} \frac{1}{t} D\left[\mathcal{P}\left(\{x(s)\}_{s=0}^{t}\right) || \mathcal{P}\left(\{x(t-s)\}_{s=0}^{t}\right)\right] \quad , \tag{S12}$$

that is valid for continuous and possibly non-Markovian stochastic processes $X(t)$. First, in practice one has access to discrete-time observations of the process $x_i \equiv X(i\Delta t)$, $i = 1, \ldots, n$, i.e., a time series containing $n = t/\Delta t$ consecutive samples of the process with sampling rate $f_{\mathrm{s}} = 1/\Delta t$. The time discretization implies a loss of information yielding a lower bound to the KL divergence rate:

$$\frac{\sigma_1}{k_{\mathrm{B}}} \geq f_{\mathrm{s}} \lim_{n\to\infty} \frac{1}{n} D[P_X(x_1, \ldots, x_n)||Q_X(x_1, \ldots, x_n)] \quad , \tag{S13}$$

where $Q_X(x_1, \ldots, x_n) = P_X(x_n, \ldots, x_1)$ is the probability to observe the reverse trajectory $(x_n, \ldots, x_1)$.

We can now apply the inequality (S11) to the right-hand side in Eq. (S13) To do that, it is necessary to find a one-to-one map $\xi_i = \xi_i(x_1, \ldots, x_n)$ that transforms the reverse time series $(x_n, \ldots, x_1)$ into a sequence of n i.i.d. random variables, that is, into a white noise. Such a transformation is usually termed *whitening transformation*.

An example of whitening transformation is the time series formed by the residuals of an autoregressive model, which is the transformation that we will use along this paper. A discrete-time stochastic process Y_i is called autoregressive of order m, AR(m), when its value at a given time is given by a linear combination of its m previous values plus a noise term. Such process is univocally determined by $m \geq 1$ real coefficients, $a_1, a_2, \ldots, a_m$, a discrete-time white noise η_i and a set of initial values $Y_1, Y_2, \ldots, Y_m$. The values of Y_i for $i > m$ are given by the linear recursion

$$Y_i = \sum_{j=1}^{m} a_j Y_{i-j} + \eta_i \quad . \tag{S14}$$

Inspired by the AR(m) process, we introduce the following one-to-one map

$$\xi_i = \begin{cases} x_i & \text{if } i \leq m \\ x_i - \displaystyle\sum_{j=1}^{m} a_j x_{i-j} & \text{if } i > m \end{cases} \quad , \tag{S15}$$

which is a linear transformation defined by a unitriangular matrix with Jacobian equal to one. With an appropriate choice of the coefficients a_j, one can get a new process $(\xi_1, \ldots, \xi_n)$ which is approximately i.i.d. A good choice is given by a maximum likelihood fit of the process to the AR(m) model. In that case, the elements ξ_i in this new time series for $i > m$ are usually called *residuals* of the original time series $(x_1, \ldots, x_n)$ with respect to the AR(m) model. Notice also that, if $(x_1, \ldots, x_n)$ is indeed a realization of the stochastic process (S14), then the residuals are i.i.d. random variables and the process $(\xi_{m+1}, \ldots, \xi_n)$ has correlations $\langle \xi_i \xi_j \rangle = \delta_{ij}$ for all $i, j > m$.

We now apply the bound (S11) to the KL divergence in the right hand side of Eq. (S13), using the transformation defined by Eq. (S15). Since the contribution of the first, possibly correlated, m values of the time series ξ_i, vanishes in the limit $n \to \infty$, we obtain the following lower bound to the KL divergence rate [Eq. (7) in the Main Text]:

$$\frac{\sigma_1}{k_{\mathrm{B}}} \geq f_{\mathrm{s}} D[p(\xi)||q(\xi)] \quad . \tag{S16}$$

We can obtain empirical estimates of $p(\xi)$ and $q(\xi)$ from a single stationary time series $(x_1, \ldots, x_n)$ as follows. We apply the transformation (S15) to *both* the original time series $(x_1, \ldots, x_n)$ and to its time reversal $(x_n, \ldots, x_1)$ obtaining, respectively, two new time series $(\xi_1^{\mathrm{F}}, \ldots, \xi_n^{\mathrm{F}})$ and $(\xi_1^{\mathrm{R}}, \ldots, \xi_n^{\mathrm{R}})$, which are stationary at least for $i > m$. The empirical PDFs obtained from the data of each series are estimations of, respectively, $p(\xi)$ and $q(\xi)$. Note that the same transformation (S15) must be applied to both the original time series $(x_1, \ldots, x_n)$ and its time reverse $(x_n, \ldots, x_1)$, but the inequality (S11) only requires uncorrelated residuals *in the reverse series*. For this purpose, we calculate the coefficients $a_1, \ldots, a_m$ by fitting the reverse time series $(x_n, \ldots, x_1)$ to the AR(m) model in Eq. (S14).

As indicated in the previous section, the inequality (S16) is tighter when the residuals are uncorrelated in the forward series as well. This is the case of the experimental series that we have analyzed (see, for instance, Fig. 2B in the Main Text) although, in principle, it is not guaranteed by this procedure. We remark that the inequality (S16) is a rigorous result if the transformation (S15) applied to the reverse time series yields an uncorrelated series

$(\xi_1^{\rm R},\ldots,\xi_n^{\rm R})$. In that case, $k_{\rm B} f_{\rm s} D[p(\xi)||q(\xi)]$ is an estimate of σ_1 with only two possible sources of error: *i)* the discrete sampling of the process $X(t)$ and *ii)* the remnant correlation time in the residuals $(\xi_1^{\rm F},\ldots,\xi_n^{\rm F})$ obtained from the forward time series.

To summarize, our theory provides an estimate $\hat{\sigma}_1$ for the KL divergence rate σ_1 which can be evaluated as follows:

1. Estimate the coefficients, $a_1,\ldots,a_m$, by fitting the *time-reversed* series $(x_n,\ldots,x_1)$ to an autoregressive AR(m) model of order $m>1$. A reasonable choice is $m=10$, but it should be tuned to minimize the correlation time in the residuals $(\xi_1^{\rm R},\ldots,\xi_n^{\rm R})$.

2. Apply the whitening transformation (S15) to the original series $(x_1,\ldots,x_n)$ and to its time reversal $(x_n,\ldots,x_1)$ to obtain, respectively, new time series $(\xi_1^{\rm F},\ldots,\xi_n^{\rm F})$ and $(\xi_1^{\rm R},\ldots,\xi_n^{\rm R})$. Note that the new processes are not each other's time reversal.

3. Obtain the empirical distributions $p(\xi)$ and $q(\xi)$ from the time series $(\xi_1^{\rm F},\ldots,\xi_n^{\rm F})$ and $(\xi_1^{\rm R},\ldots,\xi_n^{\rm R})$, respectively.

4. Calculate the KL divergence between $p(\xi)$ and $q(\xi)$

$$D[p(\xi)||q(\xi)] = \int {\rm d}\xi \, p(\xi) \ln \frac{p(\xi)}{q(\xi)} \quad , \tag{S17}$$

   which can be estimated from numerical integration of the right hand side in (S17) using the empirical normalized histograms $p(\xi)$ and $q(\xi)$. We call this estimate $\hat{\mathcal{D}}$, which is given by

$$\hat{\mathcal{D}} = \gamma \sum_i \hat{p}_i \ln \frac{\hat{p}_i}{\hat{q}_i} \quad , \tag{S18}$$

   where $\hat{p}_i = n_i^{\rm F}/(\sum_i n_i^{\rm F})$ and $\hat{q}_i = n_i^{\rm R}/(\sum_i n_i^{\rm R})$ are the empirical probabilities, obtained from the number of times $n_i^{\rm F}$ and $n_i^{\rm R}$ that the sequences $(\xi_1^{\rm F},\ldots,\xi_n^{\rm F})$ and $(\xi_1^{\rm R},\ldots,\xi_n^{\rm R})$ lie in the $i-$th bin, respectively. The sum in (S18) runs over all bins for which $n_i^{\rm F}>0$ and $n_i^{\rm R}>0$. For simplicity, we used 100 bins of equal spacing ranging from the minimum to the maximum values of the residual time series $(\xi_1^{\rm F},\ldots,\xi_n^{\rm F})$.

   The value of the estimate $\hat{\mathcal{D}}$ of the KL divergence (S17) is weighted by a prefactor $\gamma \leq 1$ defined in terms of the probability to reject the null hypothesis $p(\xi)=q(\xi)$. We use this procedure to correct the statistical bias in the estimation of the KL divergence that appears when two stochastic processes have similar statistics [31, 37]. For this purpose, we use the Kolmogorov–Smirnov (KS) statistical test under the null hypothesis $H_0 : p(\xi)=q(\xi)$ which yields a p-value $p_{\rm KS}$ for the two distributions to be equal. Here, small $p_{\rm KS}$ means that there is stronger statistical evidence in favour of the alternative hypothesis $p(\xi)\neq q(\xi)$, thus $\gamma = 1-p_{\rm KS}$ serves as a weight of irreversibility: $\gamma \simeq 0$ when it is hard to reject H_0 (reversibility) and $\gamma \simeq 1$ there is a larger statistical evidence to reject H_0.

5. Finally, our estimate of $\hat{\sigma}_1$ is thus given by the KL divergence estimate $\hat{\mathcal{D}}$ times the Boltzmann constant and the data sampling frequency:

$$\hat{\sigma_1} = k_{\rm B} f_{\rm s} \hat{\mathcal{D}} \quad . \tag{S19}$$

S3. DETAILS OF THE EXPERIMENTAL RESULTS IN FIG. 2

In this section, we describe the procedure used to estimate the bound $\sigma_{\rm tot} \geq (4.3 \pm 0.5)k_{\rm B}$/s for the experimental data shown in Fig. 2 in the Main Text. For different values of the observation time t ranging from 1.5s to 30s, we slice the time series $x_1, \ldots, x_n$ into $N \geq 1$ non-overlapping time series. We then evaluate the estimate $\hat{\sigma}_1$ given by Eq. (S19) for each of the slices following the procedure described in Sec. . The value of the irreversibility measure at each time t, denoted by $\hat{\sigma}_1(t)$ and shown in Fig. S5, is the average of the estimate $\hat{\sigma}_1$ evaluated over the different slices of length t. By fitting $\hat{\sigma}_1(t)$ as a function of time t with an exponentially-decreasing function $\hat{\sigma}_1(t) = A + B\exp(-t/\tau)$, we estimate the mean value of the irreversibility measure from the value of the fitting parameter A. Next, we estimate the error of $\hat{\sigma}_1$ (red shaded area in Fig. S5) from the standard deviation of the data points $\hat{\sigma}_1(t)$ in the long-time plateau $t \geq 5{\rm s} > \tau$, which corresponds to the stationary limit.

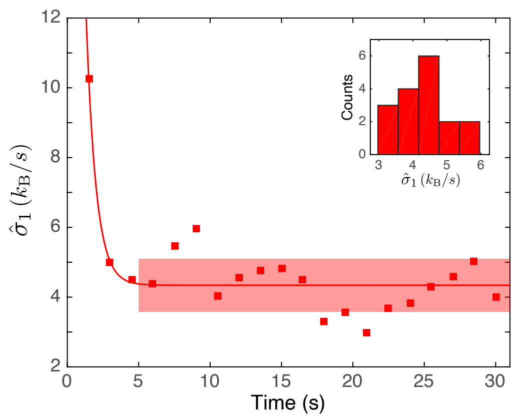

FIG. S5: Values of the irreversibility measure $\hat{\sigma}_1$ (red squares) evaluated for time traces of $t \leq \tau_{\rm exp}$, with $\tau_{\rm exp} = 30\,$s, obtained for the experimental recording shown in Fig. 2 in the Main Text. The solid line is a fit of the data to a function $\hat{\sigma}_1(t) = A + B\exp(-t/\tau)$. Parameters of the fit: $A = 4.3k_{\rm B}/s$, $B = 16k_{\rm B}$/s, $\tau = 2$s. Goodness of fit $R^2 = 0.87$. The red shaded area is centred in the long-time value A and its width equals to the standard deviation of the values $\hat{\sigma}_1(t)$ with $t \geq 5$s (see histogram in the inset), which provides the mean and the error on the steady-state value of $\hat{\sigma}_1 \geq (4.3 \pm 0.8)k_{\rm B}$/s.

S4. DETAILS OF THE EXPERIMENTAL RESULTS IN FIG. 3

In this section, we provide further details of the experimental results shown in Fig. 3 in the Main Text and additional information on the error and statistical analysis of these results.

The results in Fig. 3B of the Main text were obtained as follows. For different values of t ranging from $t_{\rm exp}/20 = 1.5$s to $t_{\rm exp}/2 = 15$s (with $t_{\rm exp} = 30$s the total time of the recording), we analyse N_t non-overlapping time series obtained by slicing the experimental time series $(x_1, \ldots, x_n)$, with $n\Delta t = t_{\rm exp}$. Here, N_t equals to $t_{\rm exp}/t$ rounded to the lowest integer. For each value of t, we obtain N_t estimates of $\hat{\sigma}_1$ as described by Eq. (S19). The data points plotted in Fig. 3B in the Main Text are given by the average of the N_t values of $\hat{\sigma}_1$, and the error bars are the standard deviation of the N_t values of $\hat{\sigma}_1$.

The results in Fig. 3C of the Main text were obtained as follows. For each of the 182 experimental recordings of hair bundle oscillations at sampling frequency $f_{\rm s} = 2.5\,$kHz, we estimate $\hat{\sigma}_1$ from the residual time series of duration $t_{\rm exp} = 30\,$s and following the procedure described in Sec. .

In Fig. S6A we show the values and error bars of the estimate $\hat{\sigma}_1$ obtained following the procedure described in Sec. . Notably, only the time series obtained from active oscillations (cyan, orange, blue and red symbols in Fig. S6A) display values of $\hat{\sigma}_1$ ($\pm$ error bars) that are larger than zero, corresponding to time-irreversible oscillations. Fig. S6B shows the value of the parameter $\gamma = 1 - p_{\rm KS}$ obtained for these 30s experimental recordings. We recall here that $p_{\rm KS}$ is the Kolmogorov–Smirnov (KS) statistic under the null hypothesis $H_0 : p = q$. This analysis reveals that recordings obtained from this set of active oscillations are not time-reversal invariant with KS p-value $p_{\rm KS} < 0.2$ (blue square in Fig. S6B), although two of the cells (green and orange symbols) show $p_{\rm KS} < 0.05$. In Fig. S6C we show the distribution of γ for the full ensemble of experimental recordings analyzed in this work. We find that in 22% of the experimental recordings, the s distributions $p(\xi)$ and $q(\xi)$ are different with $p_{\rm KS} < 0.05$, and thus $\gamma > 0.95$. The irreversibility

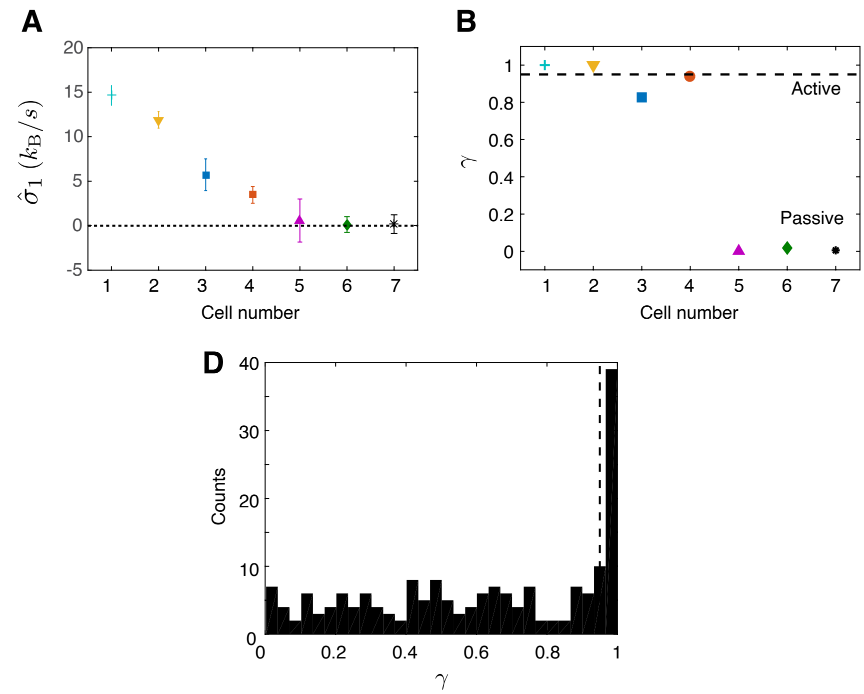

FIG. S6: **(A)** Irreversibility measure $\hat{\sigma}_1$ for the oscillations depicted in Fig. 3A of the Main Text. The value and error bars are obtained as described in Sec. . The horizontal dotted line is set to zero as a guide to the eye. **(B)** Value of the parameter $\gamma = 1 - p_{\mathrm{KS}}$ for the same oscillations, with p_{KS} the p-value of the Kolmogorov-Smirnov statistic for the distributions of the residuals ξ^{F} and ξ^{R} to be the identical. **(C)** Histogram of γ obtained from 182 experimental recordings of hair bundle oscillations each with duration of 30s. The vertical dashed line is set to a common threshold of the Kolmogorov-Smirnov parameter $\gamma = 0.95$, which corresponds to 22% of the recordings. The sampling frequency of the oscillations is $f_{\mathrm{s}} = 2.5\,\mathrm{kHz}$.

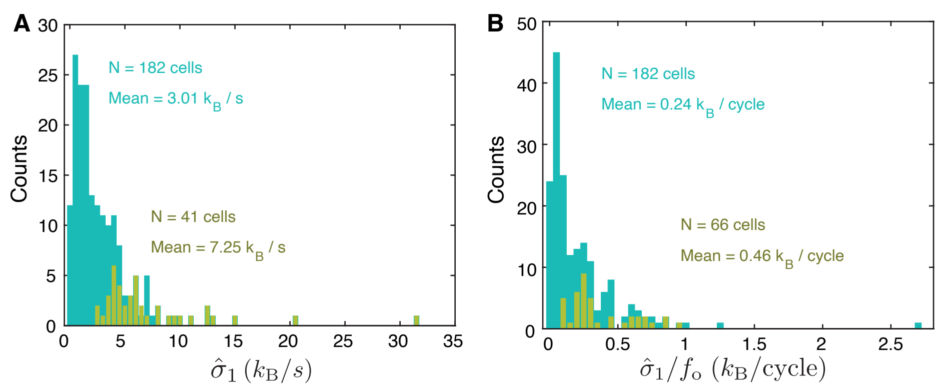

FIG. S7: Histograms of the irreversibility measure $\hat{\sigma}_1$ in units of $k_{\mathrm{B}}/\mathrm{s}$ (**A**) and in units of k_{B} per oscillation cycle (**B**). The histograms were obtained from the full ensemble of 182 oscillatory hair cells (turquoise bars) and from the sub-ensemble of 66 cells that display irreversibility in the residuals with Kolmogorov-Smirnov parameter $\gamma \geq 0.95$ (yellow bars). The sampling frequency of the oscillation is here $f_{\mathrm{s}} = 2.5\,\mathrm{kHz}$.

measure $\hat{\sigma}_1$ for this sub-ensemble of irreversible oscillations, consisting of 41 recordings, displays a distribution with mean equal to 2.4 times the mean of the full ensemble (Fig. S7A). We also compare the irreversibility measure in units of k_{B} per oscillation cycle, i.e. $\hat{\sigma}_1/f_{\mathrm{o}}$, where f_{o} is determined from a fit of the power-spectrum density (see Sec.), and show that the irreversibility of our experimental recordings is on average of the order of $0.2k_{\mathrm{B}}/\mathrm{cycle}$ ($0.5k_{\mathrm{B}}/\mathrm{cycle}$) for the full (sub-) ensemble of the cells analyzed (Fig. S7B).

Our quantification of irreversibility thus predicts that hair bundles displaying irreversibility with $p_{\mathrm{KS}} < 0.05$ produce entropy at an average rate of at least $\sim 0.5k_{\mathrm{B}}$ per oscillation cycle. Investigating the tightness of the bound $\sigma_{\mathrm{tot}} \geq$

$\hat{\sigma}_1$ is a challenging experimental task since no direct measurements of heat dissipation in spontaneous hair-bundle oscillations have yet been reported. Reference [38] reports experimental estimates of the sound power in spontaneous oto-acoustic emissions by the iguanoid lizard *Anolis sagrei*. Spontaneous oto-acoustic emissions are weak sounds that are emitted spontaneously by the ears of the animal; these sounds are though to be produced by spontaneous hair-bundle oscillations in the auditory organ of the inner ear. From these measurements, the mean power output of individual hair bundles is estimated to be on average of $141\,\mathrm{aW} = 1.41\times10^{-16}\mathrm{J/s} = 3.37\times10^4\,k_{\mathrm{B}}T/\mathrm{s}$, where $k_{\mathrm{B}}T = 4.18\times10^{-21}J$ for $T = 30°\mathrm{C}$. The oscillation frequency of lizards' hair bundles used in [38] was in the range $1-8$ kHz. Using an average oscillation frequency $f_{\mathrm{o}} = 3.5\mathrm{kHz}$, we estimate the mean power output to be on the order of $3.37\times10^4\,k_{\mathrm{B}}T/\mathrm{s}/(3.5\times10^3\mathrm{cycle/s}) \simeq 10k_{\mathrm{B}}T/\mathrm{cycle}$, i.e. 20 times larger than the average value of our measure of irreversibility (Fig. S7B). We remark here that the results presented in this section and in the Main Text are specific for the sampling frequency $f_{\mathrm{s}} = 2.5\,\mathrm{kHz}$. In the next section we will discuss how the KS p-value and our bound of entropy production depend on f_{s}.

S5. DEPENDENCY OF THE IRREVERSIBILITY MEASURE ON THE SAMPLING FREQUENCY

In this section, we analyse the dependency of our irreversibility measure on the sampling frequency f_{s}. For this purpose, we evaluate $\hat{\sigma}_1$ defined in Eq. (S19) for 30s recordings of the 182 cells that showed spontaneous oscillations at different sampling frequencies, ranging from 125Hz to 2500Hz (the latter corresponding to the data shown in Fig. 3C in the Main text). Figure S8 shows that the distribution of the irreversibility measure depends strongly on the sampling frequency of the data. Notably, the distributions shift towards higher irreversibility when the sampling frequency is reduced, until there is too much filtering $f_{\mathrm{s}} < 250\mathrm{Hz}$ such that oscillations cannot be distinguished clearly.

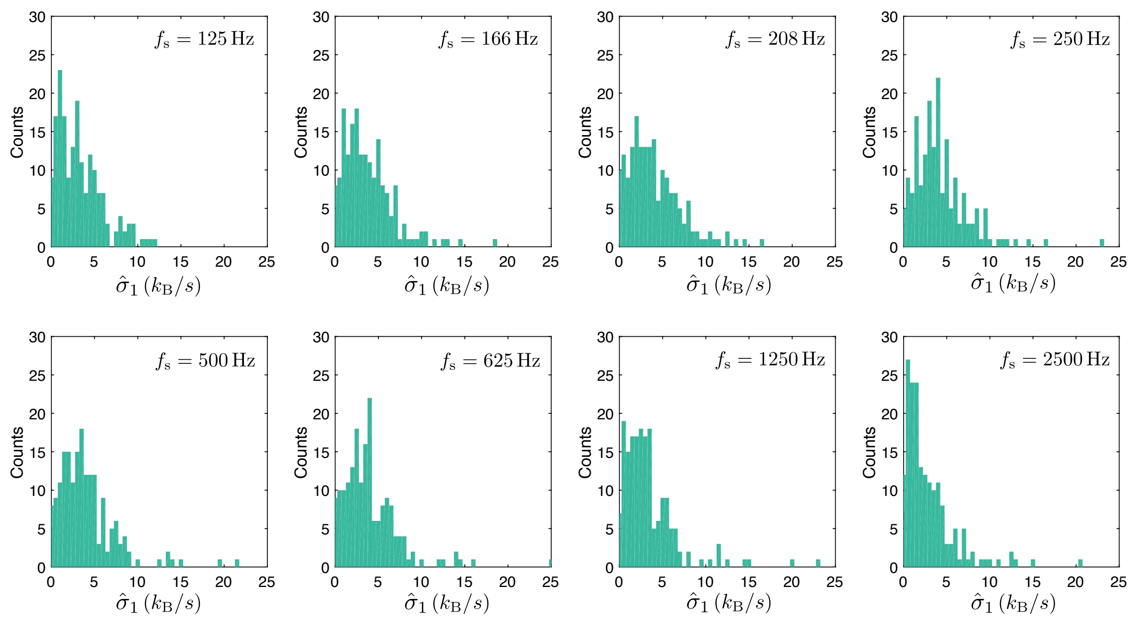

FIG. S8: Histograms of the irreversibility measure $\hat{\sigma}_1/k_{\mathrm{B}}$ for different values of the sampling frequency f_{s} indicated above each panel of the figure. All the histograms were obtained from the same ensemble of 182 oscillatory hair cells that displayed active oscillations.

In Fig. S9 we report the distributions of the parameter γ for the 182 recordings of spontaneous oscillations at different sampling frequencies. For all the analyzed cases, the distributions are right-sweked towards values of γ close to 1. Interestingly, the number of cells that display large γ (i.e. KS p-value $p_{\mathrm{KS}} < 0.05$) attains its maximum in an intermediate frequency range $\sim 200-600\mathrm{Hz}$. To gain further insight on this result, we plot in Fig. S10 box plots of the distributions of γ and of the corresponding irreversibility estimate $\hat{\sigma}_1$ as a function of the data sampling frequency. Notably, the median of γ is above 0.95 for intermediate sampling frequencies ranging from 208 to 625Hz (Fig. S10A). For values of f_s of this frequency band $208-625\mathrm{Hz}$, the median of γ is above 0.95 indicating that more than half of the cells display irreversibility with "significant" KS p-value $p_{\mathrm{KS}} < 0.05$ at those frequencies. Within this band, the median of the irreversibility measure $\hat{\sigma}_1$ decreases monotonically with f_s from $3.5\,k_{\mathrm{B}}/\mathrm{s}$ ($f_{\mathrm{s}} = 208\,\mathrm{Hz}$) to $2.6\,k_{\mathrm{B}}/\mathrm{s}$ ($f_{\mathrm{s}} = 625\,\mathrm{Hz}$).

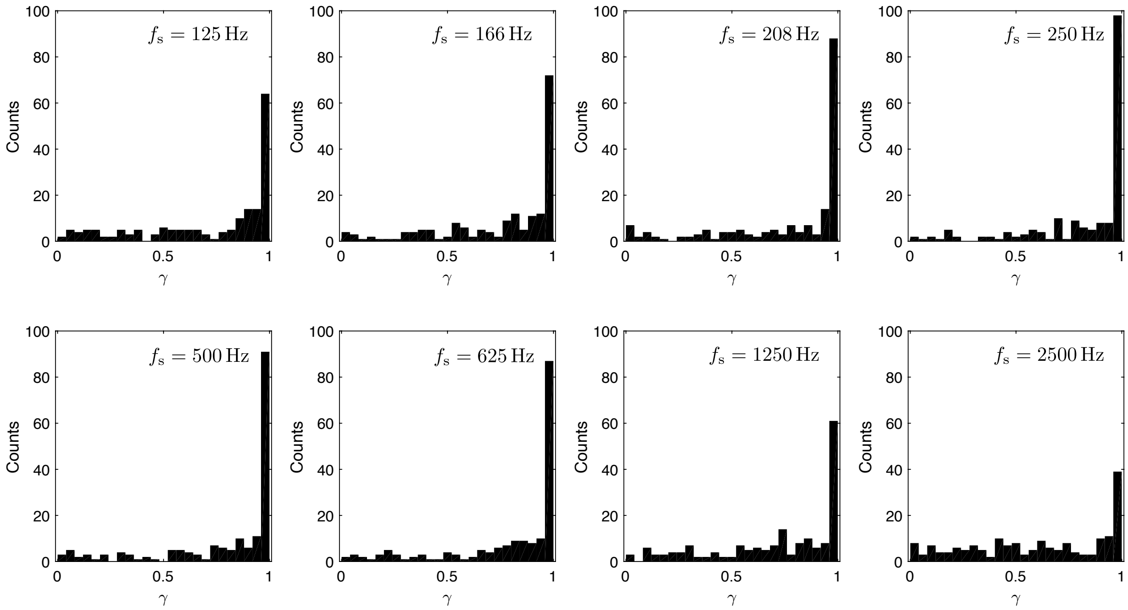

FIG. S9: Histograms of the parameter $\gamma = 1 - p_{\mathrm{KS}}$ with p_{KS} given by the Kolmogorov-Smirnov p-value for different values of the sampling frequency f_{s} indicated above each panel of the figure. All the histograms were obtained from the same ensemble of 182 oscillatory hair cells that displayed active oscillations.

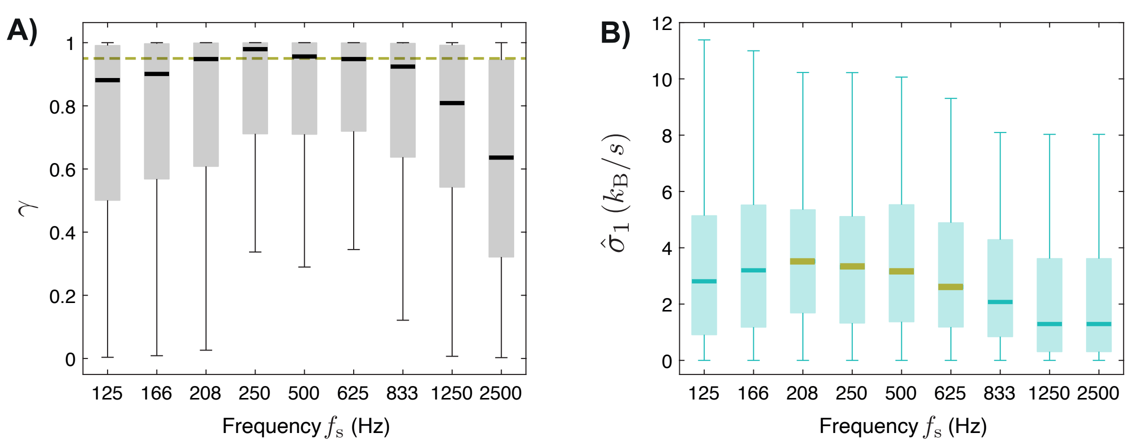

FIG. S10: Box plot of the parameter γ **(A)** and of the irreversibility measure $\hat{\sigma}_1$ **(B)** as a function of the sampling frequency obtained from recordings of the tip position of hair bundles in the entire population of 182 cells. The yellow dashed line in (A) is set to the threshold $\gamma = 0.95$ corresponding to the Kolmogorov-Smirnov p-value $p_{\mathrm{KS}} < 0.05$. In (B), we highlight (horizontal yellow thick lines) the median of the distributions of $\hat{\sigma}_1$ for which the median value of γ is larger than 0.95.

S6. LOCAL IRREVERSIBILITY MEASURE

In this section, we introduce a local irreversibility measure $\tilde{\sigma}_1(\xi)$ that provides further insights about the degree of irreversibility of a time series. For this purpose, we first note, following Shiraishi et al. [39] that the KL divergence between two univariate distributions $D[p(\xi)||q(\xi)]$ can be written as follows

$$D[p(x)||q(x)] = \int \mathrm{d}x\, p(x) \ln \frac{p(x)}{q(x)} \tag{S20}$$

$$= \int \mathrm{d}x \underbrace{\left[p(x) \ln \frac{p(x)}{q(x)} + q(x) - p(x)\right]}_{\equiv s[p(x)||q(x)] \geq 0} \quad , \tag{S21}$$

where in the second line we have used the fact that both p and q are normalized, i.e. $\int \mathrm{d}x\, p(x) = \int \mathrm{d}x\, q(x) = 1$. In Ref. [39] it was shown that the function $s[p(x)||q(x)] = p(x) \ln \frac{p(x)}{q(x)} + q(x) - p(x)$ is positive, and thus provides a local distance between two probability densities $p(x)$ and $q(x)$ i.e. at a given value of the random variable x. Following the irreversibility estimate provided by Eq. (S19) we can define the local irreversibility as

$$s_1(\xi) = k_\mathrm{B} f_\mathrm{s} \left[p(\xi) \ln \frac{p(\xi)}{q(\xi)} + q(\xi) - p(\xi)\right] \quad , \tag{S22}$$

which obeys by definition $\sigma_1 = \int \mathrm{d}\xi\, s_1(\xi)$. Figure S11 shows estimates of $s_1(\xi)$ obtained for the seven time series reported in Fig. 3(A-B) in the Main Text. The estimate $\hat{s}_1(\xi)$ is obtained by replacing $p(\xi)$ and $q(\xi)$ in Eq. (S22) by the corresponding empirical densities. Notably, active cells exhibit larger values of irreversibility than passive cells: at any value of the residual ξ of the whitening transformation, we find $\hat{s}_1^{\mathrm{act}}(\xi) \geq \hat{s}_1^{\mathrm{pass}}(\xi)$. Moreover, typical values of local irreversibility are in the range $\hat{s}_1^{\mathrm{act}}(\xi) \sim 0.1 k_\mathrm{B}/\mathrm{s}$ for such active cells and $\hat{s}_1^{\mathrm{pass}}(\xi) \sim 10^{-4} k_\mathrm{B}/\mathrm{s}$ for the passive cells, and the latter is comparable to the result obtained for the experimental noise.

We evaluate in Fig. S11 the local irreversibility measure for three representative experimental time series (Fig. S11A). We plot in Fig. S11B the residual distributions corresponding to the active cell in Fig. 2 in Main Text (blue), an active cell whose time series exhibits large jumps (red) and experimental noise (green). The active cell with larger jumps produces the most noticeable difference of the residual distributions at the tails $|\xi| \geq 0.5$. Notably, we show in Fig. S11C that the local irreversibility measure for the active cells is three orders of magnitude larger than its value for the passive oscillation, throughout all the range of values of the residuals. Furthermore, the contributions to the local irreversibility measure from central and extreme residuals are of the same order of magnitude, for both typical and atypical (large jumps) active oscilaltions.

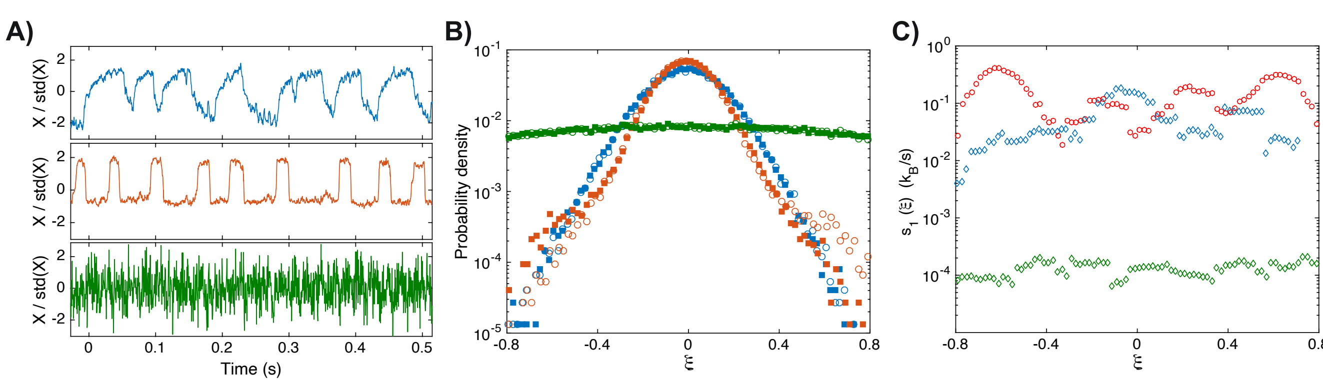

FIG. S11: **(A)** Snapshots of duration 0.5s extracted from 30s-experimental recordings of the position of the tip of two active hair bundles (top blue and middle red) and of experimental noise, normalized by the time series standard deviation. Empirical probability density (**(B)**) of the residuals $p(\xi)$ (filled squares) and $q(\xi)$ (open circles), and local irreversibility measure (**(C)**) given by Eq. (S22) for the time series partially shown in (A).

S7. QUANTIFICATION OF ENTROPY PRODUCTION IN NUMERICAL SIMULATIONS OF HAIR BUNDLE OSCILLATIONS

In this Section, we provide numerical results for the stochastic model of the ear hair bundle given by Eqs. (3-5) in the Main Text. The steady-state entropy production rate of the model is given by

$$\sigma_{\mathrm{tot}} = \frac{1}{T}\left\langle F_1 \circ \frac{\mathrm{d}X_1}{\mathrm{d}t}\right\rangle + \frac{1}{T_{\mathrm{eff}}}\left\langle F_2 \circ \frac{\mathrm{d}X_2}{\mathrm{d}t}\right\rangle \quad , \tag{S23}$$

where $F_1 = F_1(X_1, X_2)$, $F_2 = F_2(X_1, X_2)$ and $\circ$ denotes the Stratonovich product. Using the definitions of the forces in Eq. (S23) one obtains after some algebra Eq. (6) in the Main Text. In all our numerical simulations, we estimate the steady-state averages of the type

$$\left\langle F \circ \frac{\mathrm{d}X}{\mathrm{d}t}\right\rangle = \lim_{t\to\infty} \frac{1}{t}\int_0^t F(t') \circ \mathrm{d}X(t') \quad , \tag{S24}$$

for a generic force $F(t) = F(X(t), Y(t))$ from a single stationary trajectory of total duration $t_{\mathrm{sim}} = 300\,\mathrm{s}$ and sampling time $\Delta t = 1\,\mathrm{ms}$ as follows:

$$\left\langle F \circ \frac{\mathrm{d}X}{\mathrm{d}t}\right\rangle \simeq \frac{1}{t_{\mathrm{sim}}}\sum_{i=1}^{n}\left(\frac{F(t_i) + F(t_{i-1})}{2}\right)(X(t_i) - X(t_{i-1})) \quad , \tag{S25}$$

where $t_i = i\Delta t$ and $n = t_{\mathrm{sim}}/\Delta t$.

S8. ESTIMATION OF THE QUALITY FACTOR OF STOCHASTIC OSCILLATORS

We estimate the quality factor Q of spontaneous hair-bundle oscillations from numerical simulations of the hair-bundle stochastic model given by Eqs. (3-4) in the Main Text. For this purpose, we generate a single numerical simulation of duration $t_{\mathrm{sim}} = 300\,\mathrm{s}$. We then partition the simulation into 10 consecutive traces of duration $T = t_{\mathrm{sim}}/10 = 30\,\mathrm{s}$. For each of these traces $\{X_\alpha(t)\}$ $(\alpha = 1, \dots, 10)$ we compute the power spectral density as $C_\alpha(f) = (1/T)\left|\int_0^T X_\alpha(s)e^{2\pi i f t}\,\mathrm{d}t\right|^2$. We then calculate the average of the power spectral density over the 10 different traces $\tilde{C}(f) = (1/10)\sum_{\alpha=1}^{10} C_\alpha(f)$ and fit the estimate $\tilde{C}(f)$ as a function of f to the sum of two Lorentzian functions [4, 15, 45]

$$\tilde{C}(f) = \frac{A}{(f_{\mathrm{o}}/2Q)^2 + (f - f_{\mathrm{o}})^2} + \frac{A}{(f_{\mathrm{o}}/2Q)^2 + (f + f_{\mathrm{o}})^2} \quad , \tag{S26}$$

where Q is the quality factor, f_{o} is the oscillation frequency and $A > 0$ is an amplitude parameter. Figure S12 shows examples of numerical simulations for which we apply this procedure to determine the value of the quality factor by extracting the value Q from the fit of the data to Eq. (S26). Notably, Eq. (S26) reproduces power spectra of hair-bundle simulations for oscillations with values Q that are in a wide range of orders of magnitude (Fig. S12C).

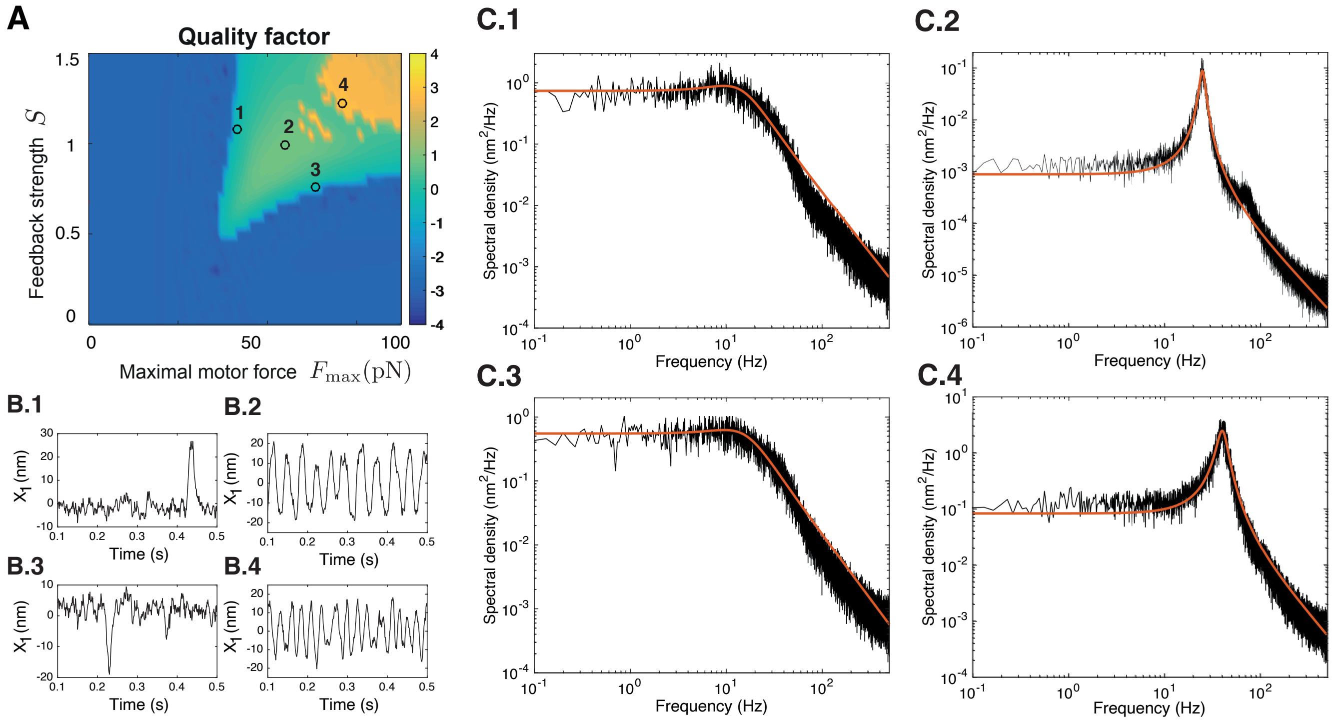

FIG. S12: Estimation of the quality factor Q from numerical simulations of the hair bundle. **(A)** Values of the quality factor Q calculated from numerical simulations of duration $t_{\mathrm{sim}} = 300\,\mathrm{s}$ for the same parameter values as in Fig. 4 in the Main Text. **(B)** Examples of 0.5-second traces of X_1 as a function of time for the parameter values indicated in A: B.1) [1 in (A)]; B.2) [2 in (A)], B.3) [3 in (A)]; B.4) [4 in (A)]. **(C)** Power spectral density (black line) of the numerical simulations with parameter values indicated with black open circles in (A). The quality factor is estimated from a fit of the power spectra to Eq. (S26) (red line). The values of Q and f_{o} extracted from the fits are: $Q = 0.5, f_{\mathrm{o}} = 7.3\,\mathrm{Hz}$ (C.1), $Q = 7, f_{\mathrm{o}} = 25\,\mathrm{Hz}$ (C.2), $Q = 0.45, f_{\mathrm{o}} = 10.6\,\mathrm{Hz}$ (C.3), $Q = 3.8, f_{\mathrm{o}} = 41.3\,\mathrm{Hz}$ (C.4).

S9. BIOPHYSICS OF MECHANOSENSORY HAIR BUNDLES

Details of the experimental procedure have been published elsewhere [2]. In short, an excised preparation of the bullfrog's (*Rana catesbeiana*) sacculus was mounted on a two-compartment chamber to reproduce the ionic environment of the inner ear. This organ is devoted to sensitive detection of low-frequency vibrations ($5-150$ Hz) of the animal's head in a vertical plane; it contains about 3000 sensory hair cells that are arranged in a planar epithelium. The basal bodies of hair cells were bathed in a standard saline solution and the hair bundles projected in an artificial endolymph. The preparation was viewed through a $\times 60$ water-immersion objective of an upright microscope. Under these conditions, spontaneous hair-bundle oscillations were routinely observed. The oscillations could be recorded by imaging, at a magnification of $\times 1000$, the top of the longest stereociliary row onto a displacement monitor that included a dual photodiode. Calibration was performed by measuring the output voltages of this photometric system in response to a series of offset displacements. Here, we analyzed 182 spontaneously oscillating hair bundles from data previously published [15].

Spontaneous hair-bundle oscillations were described by a published model of active hair-bundle motility [2] that rest on a necessary condition of negative hair-bundle stiffness, on the presence of molecular motors that actively pull on the tip links, and on feedback by the calcium component of the transduction current. Hair-bundle deflections affect tension in tip links that interconnect neighbouring stereocillia of the bundle. Changes in tip-link tension in turn modulate the open probability of mechano-sensitive ion channels connected to these links. Importantly, the relation between channel gating and tip-link tension is reciprocal: gating of the transduction channels affects tip-link tension. Consequently, channel gating effectively reduces the stiffness of a hair bundle, a phenomenon appropriately termed "gating compliance", which can result in negative stiffness if channel-gating forces are strong enough. Active hair-bundle movements result from the activity of the adaptation motors. By controlling tip-link tension, adaptation motors regulate the open probability of the mechanosensitive channels. The force produced by the motors is in turn regulated by the Ca^{2+} component of the transduction current which thus provides negative feedback on the motor force [2]. When the fixed point of this dynamical system corresponds to an unstable position of negative stiffness, the system oscillates spontaneously. The maximal force exerted by the motors F_{max} and the calcium feedback strength S are control parameters of the system and fully determine its dynamics (oscillatory, quiescent, bi-stable) [25].